Journal of Materials Chemistry C

Particle dispersion system consisting of helically assembled liquid crystalline poly(*para*-phenylene) derivatives with reproducible chiroptical properties

Journal:	*Journal of Materials Chemistry C*
Manuscript ID	TC-ART-09-2022-003747.R1
Article Type:	Paper
Date Submitted by the Author:	30-Nov-2022
Complete List of Authors:	Horie, Keita ; Ritsumeikan University, Research Organization of Science and Technology Kondo, Shunsuke; Kyoto University, Department of Polymer Chemistry Akagi, Kazuo; Ritsumeikan University, Research Organization of Science and Technology

Particle dispersion system consisting of helically assembled liquid crystalline poly(*para*-phenylene) derivatives with reproducible chiroptical properties

Keita Horie[1,2], Shunsuke Kondo[1], and Kazuo Akagi[1,2]*

[1] Department of Polymer Chemistry, Kyoto University, Katsura, Kyoto 615-8510, Japan

[2] Research Organization of Science and Technology, Ritsumeikan University, Kusatsu, Shiga 525-8577, Japan

*To whom correspondences should be addressed.

E-mail: akagi@fc.ritsumei.ac.jp

Abstract

Liquid crystalline poly(*para*-phenylene) [LC-PPP] derivatives bearing a cyanobiphenyl moiety on the side chain and axially chiral binaphthyl derivatives were synthesized. To prevent artefacts arising from intrinsic anisotropies of the main and side chains of the LC-PPP derivative in circular dichroism (CD) and circularly polarized luminescence (CPL) spectra, a particle dispersion system was constructed from an LC-PPP derivative and an axially chiral binaphthyl derivative as a chiral dopant. Use of this particle dispersion system resulted in good reproducibility for chiroptical measurements and no discernible artefacts in either the CD or CPL spectra, enabling us to quantitatively analyse the chiroptical properties of the LC-PPP derivative. We elucidated the overall mechanism by which the axially chiral binaphthyl dopant induced helicity in the LC-PPP derivative.

1. Introduction

Various approaches have been reported for the synthesis of materials with circularly polarized luminescence (CPL). For example, chiral moieties can be introduced into molecules, polymers, or coordinated compounds or chiral compounds can be doped into achiral/racemic compounds to create helical structures that induce chirality.[1-4] Using polymers to construct CPL devices enables the facile fabrication of films by casting techniques, whereby even films with large areas can be produced. Polymers can also be used to facilitate the fabrication of devices used in organic light emitting diodes and solar batteries. Thus far, we have used various approaches to synthesize conjugated polymers bearing CPL functions, i.e., (i) synthesis of aromatic conjugated polymers with side chains bearing chiral moieties,[5-9] (ii) exploitation of intermolecular electrostatic interactions to construct a helically stacked assembly between achiral conjugated polymers bearing ionic side chains and counterionic chiral compounds,[10,11] (iii) synthesis of liquid crystalline *di*-substituted polyacetylene derivatives with chiral side chains[12], and (iv) exploitation of selective reflection/transmission functions of chiral nematic

liquid crystals to amplify the CPL for chiral fluorescent conjugated polymers and even control the CPL helicity by temperature change. [13,14] It is highly interesting that (iii) and (iv) afford CPLs with a high dissymmetry factors (g_{lum}) on the order of 10^{-1} and 10^{0}, respectively. Note that the term CPF was previously used in this field instead of CPL simply because CPF directly indicates fluorescence with circular polarization. The term CPL is currently used to include circularly polarized luminescence arising from fluorescence and phosphorescence.

Delocalized π-electrons in the main chain of conjugated polymers result in significant electrical and optical properties, such as electrical conductivity, luminescence, and photoharvesting

behaviour, whereby these polymers are regarded as candidate materials for organic optoelectronic devices.[15-24] Helical conjugated polymers have been attracting interest because of unique chiroptical functions[25-32], such as CPL, as well as circular dichroism (CD). These helical conjugated polymers have intrachain-twisted, intrachain-spiral, or interchain-helical π-stacked structures. Among these structures, the interchain-helical π-stacked structure can effectively enable self-assembly of aromatic conjugated polymers (ACPs) into an interchain helix and even a higher-order supramolecular structure with potentially amplified chiroptical properties.

It is well known that liquid crystallinity can be effectively exploited to control high-order polymer structures.[33-36] Polymers bearing a liquid crystalline (LC) moiety spontaneously align into polydomains through the orientation of the LC moiety. Furthermore, the incorporation of chiral moieties or chiral dopants into LC polymers results in helical arrangement into a higher-order hierarchical structure. We previously reported that LC polyacetylene derivatives[12], *mono*- and *di*-substituted LC-PPP derivatives[37] and LC-copolymers containing *mono*-substituted phenylene and ethylenedioxythiophene[38] exhibit circular polarization in absorption and/or luminescence as a result of helical structures induced upon addition of chiral binaphthyl dopants. However, both the LC moieties bearing mesogenic cores and rigid aromatic conjugated main chains have intrinsic anisotropies that manifest as linear dichroism (LD) and linear birefringence (LB) in the solid-state. These anisotropies produce artefacts in CD spectra.[37-41] Therefore, special care should be taken when making CD measurements of films. In addition, the presence of artefacts deteriorates the reproducibility of measurements of optical properties of films.

There have been many reports of helical assemblies formed in solution, e.g., aggregates of ACPs bearing chiral side chains.[42-46] In these studies, ACPs were found to aggregate in solution

upon the addition of a poor solvent. However, this method cannot be used to transfer chirality from chiral molecules to ACPs. This inability to transfer chirality results from ACPs easily π-stacking into an aggregate before associating with chiral molecules. Conventional methods, such as emulsion polymerization[47,48] and seed polymerization[49-51], are used to prepare aggregates and/or particles of ACPs but under restricted conditions. Recently, a simple and versatile method called "self-organized precipitation (SORP)" was developed to prepare polymer nano- or microsized particles.[52-54] The SORP method can be used to prepare a particle dispersion system composed of size-controlled polymers from a mixed solution of a volatile good solvent and a nonvolatile poor solvent.

Herein, an LC-PPP derivative was synthesized by introducing a cyanobiphenyl mesogenic moiety into the side chain of PPP. Subsequently, axially chiral binaphthyl derivatives [(*R*)-/(*S*)-D1] were synthesized, as shown in Fig. 1, for use as chiral dopants. As both the PPP main chain and the LC side chain are intrinsically anisotropic, we prepared a particle dispersion system from LC-PPP to prevent the occurrence of artefacts in CD and CPL spectra. As dispersed particles can freely migrate and rotate, the linear anisotropies were expected to mutually cancel even though the individual particles have LD and LB.

(Fig. 1)

2. Results and Discussion

2-1. Experimental

The synthesis routes for the chiral dopant D1 and LC-PPP are shown in Fig. 1. The helical twisting power (β) value of D1 was 42.0 μm^{-1} at 25 C°. The number average (M_n) and weight average (M_W)

molecular weights and polymer dispersion index (PDI) are summarized in Table 1. Polarizing optical microscopy (POM) analysis revealed that LC-PPP has a nematic LC phase. Fig. 2 shows the LC phase exists in the 95−160 °C temperature range under both the heating and cooling, indicating LC-PPP has an enantiotropic nature.

(Table 1 and Fig. 2)

The LC phase of LC-PPP was also investigated through X-ray diffraction (XRD) measurements. Fig. 3 shows the XRD pattern has a single broad diffraction peak in the wide angle region, typical of a nematic LC phase. The optical properties of the LC-PPP solution in tetrahydrofuran (THF) and the D1 solution in $CHCl_3$ were measured in ultraviolet–visible (UV−vis) absorption, photoluminescence (PL), and CD experiments (Figs. S1 and S2).

(Fig. 3)

Fig. 4 is a schematic of the SORP method used to prepare the polymer dispersion systems. First, mixtures with molar ratios of LC-PPP:D1 ranging from 100:1 to 100:10 were prepared in THF (a good solvent, 2 mL). Subsequently, pure water (as a poor solvent, 5 mL) was dropped into the mixture at a rate of 1.1 mL/min under stirring. Then, the solution was gradually heated at 25 °C under atmospheric pressure for 2 days. After the good solvent had been completely evaporated, the mixture containing LC-PPP and D1 precipitated as particles dispersed in water. However, for high polymer concentrations in the THF solution (e.g., 1.0×10^{-4} M), LC-PPP precipitated during the

addition of water or after evaporation of THF because PPP aggregated easily. Therefore, we screened various polymer concentrations in the THF solution and found ca. 4.5×10^{-5} M to be an appropriate concentration. The preparation conditions for the polymer dispersion systems are summarized in Table 2.

(Fig. 4 and Table 2)

Dynamic light scattering (DLS) measurements indicated that the dispersed particles had average diameters of approximately 200–300 nm, and large size dispersities of 40–60% (Table S1). As previously mentioned, PPP polymers tend to aggregate, and the equilibrium between random coils and nuclei (which may be a driving force for the formation of homogeneous nuclei[38]) is not stable. Therefore, it can be argued that the size of nuclei varies widely, resulting in wide size distributions. Fig. 5 shows scanning electron microscopy (SEM) images of the polymer systems containing spherical aggregates with diameters of several tens or one hundred nanometres. The SEM results are not consistent with the average diameters determined by DLS but show that the particles are aggregated in water.

(Fig. 5)

Fig. 6 shows the UV–vis, CD, PL and CPL spectra for the systems of LC-PPP and a chiral dopant. The spectra for all the systems exhibited PL bands at 422 nm, which correspond to the π*-π transitions of the PPP conjugated backbone. The CPL spectra of the systems exhibited Cotton effects in the region of the π*-π transition of the PPP main chains, implying helical π-stacking of

the PPP main chains. The signs of the Cotton effects are strictly determined by the (*R*)- or (*S*)-configuration of the chiral dopant. The CPL intensity increased with the quantity of the chiral dopant. The absolute values of the luminescence dissymmetry factor (g_{lum}) evaluated from the CPL spectra were relatively large, i.e., on the order of 10^{-2}, for all the systems except for System S1 (which had a g_{lum} of -4.7×10^{-3}) (Table 3). The signs of Cotton effects in CD spectra were reversed in accordance with the configuration of D1, and the CD intensity varied with the quantity of D1. Table 3 also shows that the absorption dissymmetry factors (g_{abs}) evaluated from the CD spectra were on the order of 10^{-2}. Here, it is worth noting that the LC-PPP film annealed after doping gave a larger g_{lum} value up to 0.23 when 2,2',6,6'-*tetra*-substituted chiral binaphthyl compound bearing a larger helical twisting power (β □88~102) than that of D1 (β □42) was used as a chiral dopant[37,55]. The systematic investigation of the annealing effect on LC-PPP film and the dependence of dissymmetry factor on helical twisting power of chiral dopant will be reported in the near future[55].

(Fig. 6 and Table 3)

The Cotton effects in the CD spectra were observed over a wide wavelength region ranging from approximately 250 nm to 400 nm. The UV–vis absorption bands appeared at shorter wavelengths of 305 nm, corresponding to π-π* transitions of the PPP main chains. This effect results from the overlap of the band of the PPP main chain with that of the LC moiety of the side chain. Table 4 shows the fabricated particle dispersion systems containing 2,5-dichlorobenzene bearing LC substituents (labelled LC monomer M1 (see Fig. 1)) and D1 as a chiral dopant under the same conditions as the LC-PPP systems. The CD spectra of the particle dispersion systems of M1 were

similar to those of the LC-PPP systems, especially from 250 nm to 300 nm, indicating that the bands at wavelengths of 250-300 nm arise from CD induced by D1 in the LC moiety of the side chain. To counteract the overlap between bands, we obtained difference spectra by subtracting the UV−vis and CD spectra for the M1-S system from those of the S10 system. The difference spectra shown in Fig. 7 exhibit an absorption band at 351 nm and a CD band bearing the bisignate Cotton effect near 350 nm. The absorption band at 351 nm can be attributed to π-π* transitions of the PPP main chain. Thus, it can be argued that the bisignate Cotton effect at this wavelength originated from the interchain helical π-stacked PPP main chains. Fig. 7 shows that the spectrum of LC-PPP with added (*S*)-D1 exhibits negative and positive Cotton effects at long ($\lambda \approx 350$ nm) and short wavelengths ($\lambda \approx 330$ nm), respectively, indicating the left-handed (*M*) helicity of the PPP main chains[56] (also see Fig. S5) .

(Fig. 7 and Table 4)

Next, we investigated the intrachain and interchain helicity induced in the LC-PPP. Hereafter, we refer to the (*S*)-configuration for simplicity, unless otherwise stated. First, to elucidate the interchain helicity of the LC side chains, we performed a contact test between the M1/D1 mixture and an LC standard bearing left-handedness (cholesteryl oleyl carbonate), where the results are shown in Fig. 8. The discontinuous boundary between the M1/(*R*)-D1 mixture and the LC standard indicated that the mixture has the same right-handedness (*P*-helicity) as the mixture of LC-PPP and (*R*)-D1. By contrast, the continuous boundary between the M1/(*S*)-D1 mixture and the LC standard indicated that the mixture has the same left-handedness (*M*-helicity) as the mixture of LC-PPP and (*S*)-D1.

(Fig. 8)

Subsequently, we examined the intrachain and interchain helicity induced in the PPP main chain. In a previous study, we analysed the relationship between the intrachain and interchain helicity of phenylene rings in helical poly(*meta*-phenylene) bearing a superhelix structure.[57] Namely, the interchain helicity of phenylene rings should be opposite to the intrachain helicity because opposite helical handedness for the intrachain twisted structure and interchain helically π-stacking structure enables the formation of a stable π-stacked structure (Figs. S6 and S7). Consequently, the interchain helicity of the PPP main chain of LC-PPP doped with (*S*)-D1 should be left-handed (*M*-helicity) when the intrachain helicity of the PPP main chain is right-handed (*P*-helicity). Therefore, the CD and CPL spectra of LC-PPP doped by (*S*)-D1 exhibit Cotton effects.

Zimmermann et al.[58,59] showed that binaphthyl dopants induce intramolecular helicity for cyanobiphenyl structures in oriented nematic liquid crystals. However, the process by which this intramolecular helicity generates intermolecular helicity in chiral nematic liquid crystals has not yet been clarified. Nevertheless, it is possible to discuss the process of developing intermolecular helicity from the experimental results. We have shown that the introduction of a structure similar to the mesogen group of a nematic liquid crystal at the 6,6'-position of the binaphthyl ring significantly increases the helical twisting power, even though the mesogen unit with a phenyl substituent or a long alkyl spacer remains almost unchanged[60]. Furthermore, we have shown that the introduction of a similar structure at the 4,4'-position gives no noticeable change in the helical twisting power[61]. Therefore, it can be inferred that in nematic liquid crystal compounds, the

structure of the two naphthalene rings, which are easily oriented in the long-axis direction, greatly affects the helical twisting power. It is therefore natural to assume that when binaphthyl acts as a chiral dopant, the naphthalene rings are predominantly coordinated so that their long-axis direction is parallel to the nematic direction. We have previously discussed similar coordination states in helical structures of nematic liquid crystals and helical polyacetylenes[62]. Fig. 9 shows a schematic of the helically assembled structure of LC-PPP and (*S*)-D1.

(Fig. 9)

The helicity transfer between the chiral dopant and LC-PPP can be summarized as follows. First, the right-handed helicity of the chiral dopant (*S*)-D1 is transferred to the phenylene rings of the PPP main chain and/or mesogenic biphenyl moiety of the side chain in LC-PPP through intermolecular π−π* interactions, resulting in the same handedness for the LC-PPP as for the chiral dopant D1. Namely, (*S*)-D1 with *M*-helicity induces an intermolecular *M*-helicity in the phenylene rings of the LC-PPP. Second, the intermolecular *M*-helicity in the phenylene rings of the PPP main chains is preferentially assembled with the opposite intramolecular *P*-helicity, as shown in Fig. 10. Fig. 11 shows the helical structures induced by the chiral dopant (*S*)-D1 in LC-PPP, where the PPP main chains and the LC side chains are designated as parallel on the basis of a previous report[63] (see Fig. 3).

(Figs. 10 and 11)

The analysis presented above was based on difference spectra obtained by subtracting the spectrum of the M1-S system from that of the S10 system. It was only possible to carry out this analysis after confirming the reproducibility of the spectra. Systems R10, S1, S2, S5, and S10 were fabricated again under the same conditions, and the reproducibility was confirmed in terms of the optical properties and average diameters of the particles (Figs. S8 and S9). It is important to emphasize that for all the investigated systems, there were no significant differences among measurements and no artefacts were observed in the CD and CPL spectra. Therefore, the particle dispersion system can be used to measure circular polarization properties without artefacts originating from macroscopic anisotropy and with satisfactory reproducibility.

3. Conclusion

We synthesized an LC-PPP derivative with a cyanobiphenyl-based LC side chain. Considering that both the main and side chains have macroscopic anisotropy, we fabricated particle dispersion systems containing the LCPPP derivative and a chiral dopant to prevent the appearance of artefacts in CD and CPL spectra. The chiroptical spectra of the particle dispersion systems did not contain discernible artefacts and exhibited good reproducibility. We were thus able to quantitatively analyse the circularly polarized optical properties of the material despite overlap between the absorption wavelengths of the main and side chains. The relatively high g_{abs} and g_{lum} values (on the order of 10^{-2}) in the CD and CPL spectra, respectively, were well reproduced. We elucidated the helicity induced by an axially chiral binaphthyl dopant in the LC side chain and main chain of the LCPPP derivative. Hence, the particle dispersion system can be used to perform a 'semiquantitative' study of the aggregated state in solution. This application of this system can be extended beyond polymers or polymer mixtures to oligomers and low-molecular-weight compounds.

Electronic Supplementary Information (ESI) available: Materials, measurements, and synthetic procedures.

Conflicts of interest

The authors declare no competing interest.

Acknowledgments

The authors are grateful to Dr. H. Iida for his valuable cooperation in synthesis and spectroscopic

measurements, to Mr. S. Yoshida for his drawing of the schematic helicity transfer, and to Dr. K. Watanabe for his helpful discussion. This work was supported by Grants-in-Aid for Science Research (No. 20H02818) from the Ministry of Education, Culture, Sports, Science and Technology (MEXT), Japan, and by JST, CREST grant number JPMJCR2001, Japan.

References

1 K. Akagi, G. Piao, S. Kaneko, K. Sakamaki, H. Shirakawa and M. Kyotani, *Science,* 1998, **282**, 1683-1686.

2 K. Akagi, *Chem. Rev.,* 2009, **109**, 5354-5401.

3. M. Goh, S. Matsushita and K. Akagi, *Chem. Soc. Rev.*, 2010, **39**, 2466-2476.

4. K. Akagi, *Bull. Chem. Soc. Jpn.,* 2019, **92**, 1509-1655.

5 I. Osaka, A. Nakamura, Y. Inoue and K. Akagi, *Trans. Mat. Res. Soc. Jpn.*, 2002, **27**, 567–570.

6 S. Yorozuya, I. Osaka, A. Nakamura, Y. Inoue and K. Akagi, *Synth. Met.*, 2003, **135-136**, 93–94.

7 H. Hayasaka, K. Tamura and K. Akagi, *Trans. Mat. Res. Soc. Jpn.,* 2006, **32**, 395–398.

8 H. Hayasaka, T. Miyashita, K. Tamura and K. Akagi, *Adv. Funct. Mater.,* 2010*,* **20**, 1243–1250.

9 K. Watanabe, I. Osaka, S. Yorozuya and K. Akagi, *Chem. Mater.,* 2012, **24**, 1011–1024.

10 K. Watanabe, H. Iida and K. Akagi, *Adv. Mater.*, 2012, **24**, 6451–6456.

11 K. Watanabe, Z. Sun and K. Akagi, *Chem. Mater.*, 2015, **27**, 2895–2902.

12 B. A. San Jose, S. Matsushita and K. Akagi, *J. Am. Chem. Soc.*, 2012, **134**, 19795–19807.

13 B. A. San Jose, J. Yan and K. Akagi, *Angew. Chem. Int. Ed.*, 2014, **53**, 10641-10644.

14 J. Yan, F. Ota, B. A. San Jose, and K. Akagi, *Adv. Funct. Mater.*, 2017, **27**, 1604529 (1-10).

15 J. H. Burroughes, D. D. C. Bradley, A. R. Brown, R. N. Marks, K. Mackay, R. H. Friend, P. L. Burn and A. B. Holmes, *Nature,* 1990, **347**, 539-541.

16 R. H. Friend, R. W. Gymer, A. B. Holmes, J. H. Burroughes, R. N. Marks, C. Taliani, D. D. C.; Bradley, D. A. Dos Santos, J. L. Bredas, M. Logdlund and W. R. Salaneck, *Nature,* 1999, **397**, 121-128.

17 D. T. McQuade, A. E. Pullen and T. M. Swager, *Chem. Rev.,* 2000, **100**, 2537-2574.

18 G. Li, V. Shrotriya, J. S. Huang, Y. Yao, T. Moriarty, K. Emery and Y. Yang, *Nat. Mater.,* 2005, **4**, 864-868.

19 Y. Kim, S. Cook, S. M. Tuladhar, S. A. Choulis, J. Nelson, J. R. Durrant, D. D. C. Bradley, M. Giles, I. Mcculloch, C. S. Ha and M. Ree, *Nat. Mater.,* 2006, **5**, 197-203.

20 S. Guenes, H. Neugebauer and N. S. Sariciftci, *Chem. Rev.,* 2007, **107**, 1324-1338.

21 T. Masuda, *J. Polym. Sci., Part A: Polym. Sci.,* 2007, **45**, 165-180.

22 S. W. Thomas, G. D. Joly and T. M. Swager, *Chem. Rev.,* 2007, **107**, 1339-1386.

23 C. V. Hoven, A. Garcia, G. C. Bazan and T.-Q. Nguyen, *Adv. Mater.,* 2008, **20,** 3793-3810.

24 J. Liu, J. W. Y. Lam and B. Z. Tang, *Chem. Rev,.* 2009, **109**, 5799-5867.

25 E. Yashima, K. Maeda, H. Iida, Y. Furusho and K. Nagai, *Chem. Rev.,* 2009, **109**, 6102-6211.

26 K. Watanabe and K. Akagi, *Sci. Technol. Adv. Mater.,* 2014, **15**, 44203-444224.

27 M. Verswyvel and G. Koeckelberghs, *Polym. Chem.,* 2012, **3**, 3203-3216.

28 L. A. P. Kane-Maguire and G. G. Wallace, *Chem. Soc. Rev.,* 2010, **39**, 2545-2576.

29 Y. Nagata, K. Takagi and M. Suginome, *J. Am. Chem. Soc.,* 2014, **136**, 9858-9861.

30 H. Sogawa, Y. Miyagi, M. Shiotsuki and F. Sanda, *Macromolecules,* 2013, **46**, 8896-8904.

31 M. Gon, Y. Morisaki and Y. Chujo, *J. Mater. Chem. C*, 2015, **3**, 521-529.

32 H. Kawashima, K. Kawabata and H. Goto, *J. Mater. Chem. C,* 2015, **3**, 1126-1133.

33 V. V. Tsukruk, V. V. Shilov and Y. S. Lipatov, *Acta. Polym.,* 1985, **36**, 403-412.

34 V. Shibaev, A. Bobrovsky and N. Boiko, *Prog. Polym. Sci.,* 2003, **28**, 729-836.

35 S. J. Zhang, E. M. Terentjev and A. M. Donald, *Langmuir,* 2005, **21**, 3539-3543.

36 A. Yoshizawa, *Polym. J.,* 2012, **44**, 490-502.

37 H. Iida, A. Nakamura, Y. Inoue and K. Akagi, *Synth. Met,* 2000, **135-136**, 91-92.

38 Y. S. Jeong and K. Akagi, *J. Mater. Chem.,* 2011, **21**, 10472-10481.

39 Y. Shindo and Y. Ohmi, *J. Am. Chem. Soc.,* 1985, **107**, 91-97.

40 Y. Shindo, M. Nishio and S. Maeda, *Biopolym.,* 1990, **30**, 405-413.

41 Y. Shindo and M. Nishio, *Biopolym.,* 1990, **30**, 25-31.

42 M. M. Bouman , E. E. Havinga , R. A. J. Janssen and E. W. Meijer, *Mol. Cryst. Liq. Cryst.,* 1994, **256**, 439-448.

43 R. Fiesel and U. Scherf, *Acta. Polym.,* 1998, **49**, 445-449.

44 X. Y. Zhao and K. S. Schanze, *Langmuir,* 2006, **22**, 4856-4862.

45 M. Vangheluwe, T. Verbiest and G. Koeckelberghs, *Macromolecules,* 2008, **41**, 1041-1044.

46 C. Resta, S. Di Pietro, M. M. Elenkov, Z. Hamersak, G. Pescitelli and L. Di Bari, *Macromolecules,* 2014, **47**, 4847-4850.

47 Y. Chevalier, *Current Opinion in Colloid & Interface Science,* 2002, **7**, 3-11.

48 D. Dupin, S. Fujii, S. P. Armes, P. Reeve and S. M. Baxter, *Langmuir,* 2006, **22**, 3381-3387.

49 I. Cho and K. W. Lee, *J. Appl. Polym. Sci.,* 1985, **30**, 1903-1926.

50 M. Okubo, M. Shiozaki, M. Tsujihiro and Y. Tsukuda, *Colloid Polym. Sci.,* 1991, **269**, 222-226.

51 O. Karlsson, H. Hassander and B. Wesslen, *J. Appl. Polym. Sci.,* 1997, **63**, 1543-1555.

52 H. Yabu, T. Higuchi, K. Ijiro and M. Shimomura, *Chaos,* 2005, **15**, 047505.

53 H. Yabu, K. Akagi and M. Shimomura, *Synth. Met.*, 2009, **159**, 762-764.

54 H. Yabu, *Bull. Chem. Soc. Jpn.,* 2012, **85**, 265-274.

55 K. Horie, H. Iida and K. Akagi, unpublished results.

56 N. Berova, K. Nakanishi and R. Woody, Eds, *Circular Dichroism: Principles and Application*, 2nd ed., Wiley-VCH, New York, 2000.

57 T. Mori and K. Akagi, *Macromolecules,* 2013, **46**, 6699-6711.

58 G. Gottarelli, M. Hibert, B. Samori, G. Solladie, G. P. Spada and R. Zimmermann, *J. Am. Chem. Soc.,* 1983, **105**, 7318-7321.

59 G. Gottarelli, G. P. Spada, R. Bartsch, G. Solladie and R. Zimmermann, *J. Org. Chem.,* 1986, **51**, 589-592.

60 M. Goh and K. Akagi, *Liq. Cryst.*, 2008, **35**, 953-965.

61 M. Goh, J. Park, Y. Han, S. Ahn and K. Akagi, *J. Mate. Chem.*, 2012, **22**, 25011-25018.

62 T. Mori, M. Kyotani and K. Akagi, *Macromolecules*, 2008, **41**, 607-613.

63 J. Oguma, R. Kawamoto, H. Goto, K. Itoh and K. Akagi, K. *Synth. Met.* 2001, **119**, 537-538.

Captions of Figure and Table:

Fig. 1 Synthesis routes for the chiral dopant D1, monomer, and LC-PPP.

Fig. 2 (Upper) POM image at 150 °C and (lower) phase transition temperatures determined by POM observation of LC-PPP.

Fig. 3 (Upper) XRD pattern of LC-PPP in the annealed film and (lower) schematic of the nematic phase of LC-PPPs.

Fig. 4 Preparation of particle dispersion systems by the SORP method.

Fig. 5 SEM images of particles in (a) R10, (b) S1, (c) S2, (d) S5, and (e) S10.

Fig. 6 (a) UV−vis and CD spectra and (b) PL and CPL spectra of the polymer-particle dispersion systems.

Fig. 7 UV−vis and CD spectra of the S10 and M1-S systems and the difference spectrum for the PPP main chain obtained by subtracting the M1-S spectrum from the S10 spectrum.

Fig. 8 Contact test between the mixture of LC molecule and chiral dopant (*R*)-/(*S*)-D1 and cholesteryl oleyl carbonate used as a left-handed LC standard.

Fig. 9 Schematic of the mechanism of helicity transfer from (*S*)-D1 to the LC-PPP.

Fig. 10 Schematics showing helicity induced by the chiral dopant (*R*)-/(*S*)-D1 in different parts of LC-PPP.

Fig. 11 Schematics showing helicity induced by the chiral dopant (*R*)-/(*S*)-D1 to the entire LC-PPP.

Table 1 Optical properties of LC-PPP and the chiral dopant (*R*)-/(*S*)-D1 in $CHCl_3$ (2.0×10^{-5} M).

Table 2 Conditions for the preparation of particle dispersion systems containing LC-PPP and (*R*)-/(*S*)-D1 by the SORP method.

Table 3 Optical properties of particle dispersion systems, including LC-PPP and the chiral dopant (*R*)-/(*S*)-D1.

Table 4 Conditions for the preparation of particle dispersion systems containing the M1 monomer and (*R*)-/(*S*)-D1 by the SORP method.

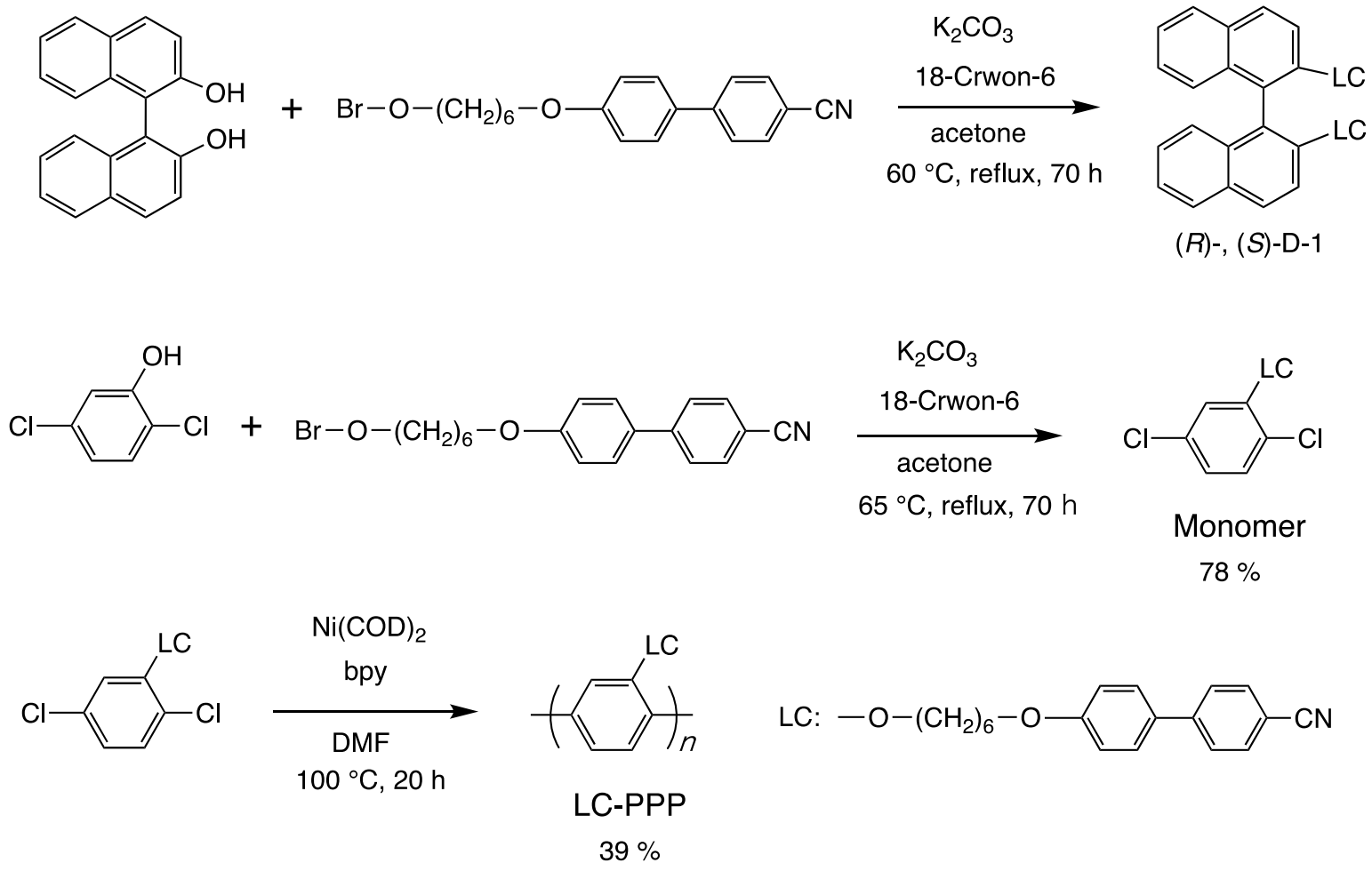

Fig. 1 Synthesis routes for the chiral dopant D1, monomer, and LC-PPP.

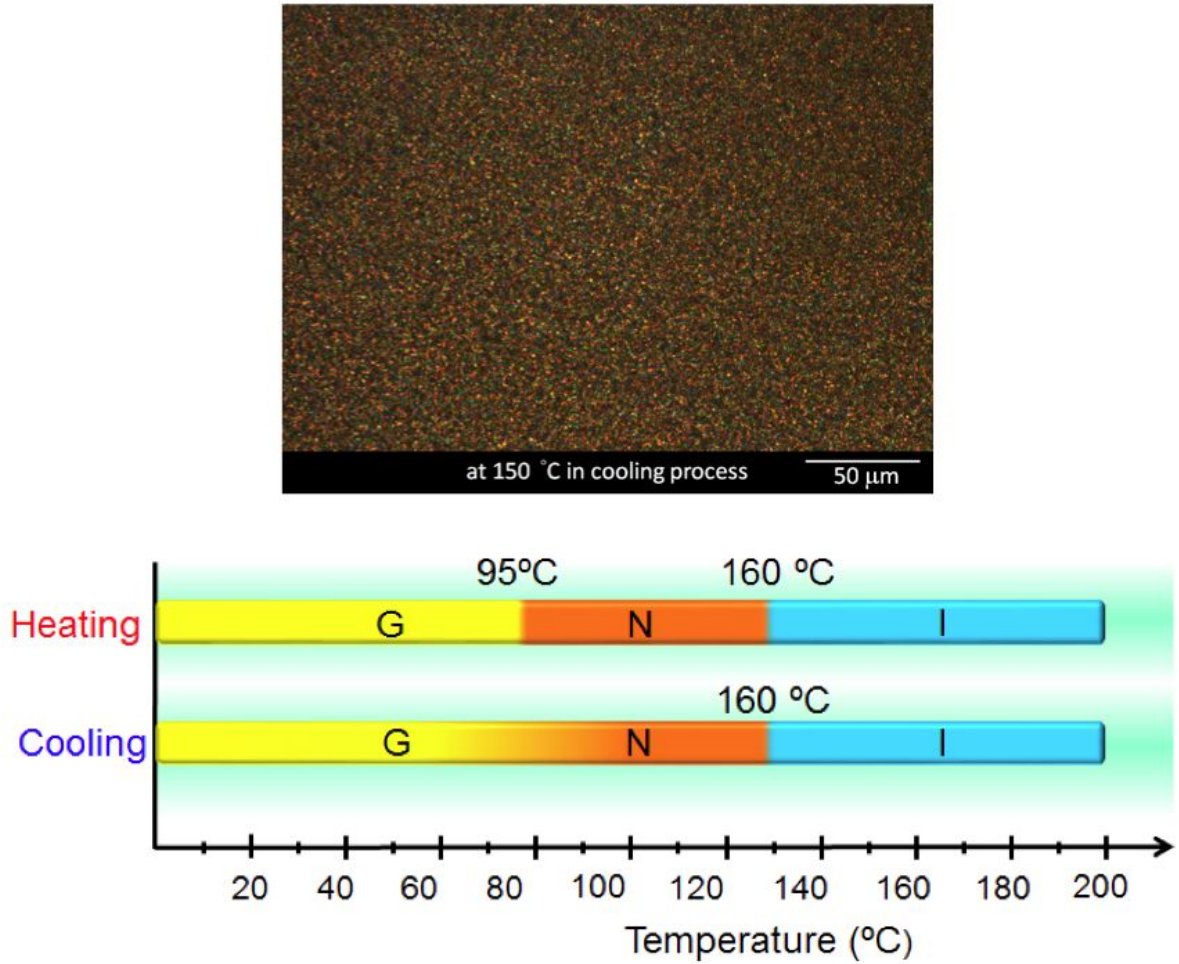

Fig. 2 (Upper) POM image at 150 °C and (lower) phase transition temperatures determined by POM observation of LC-PPP.

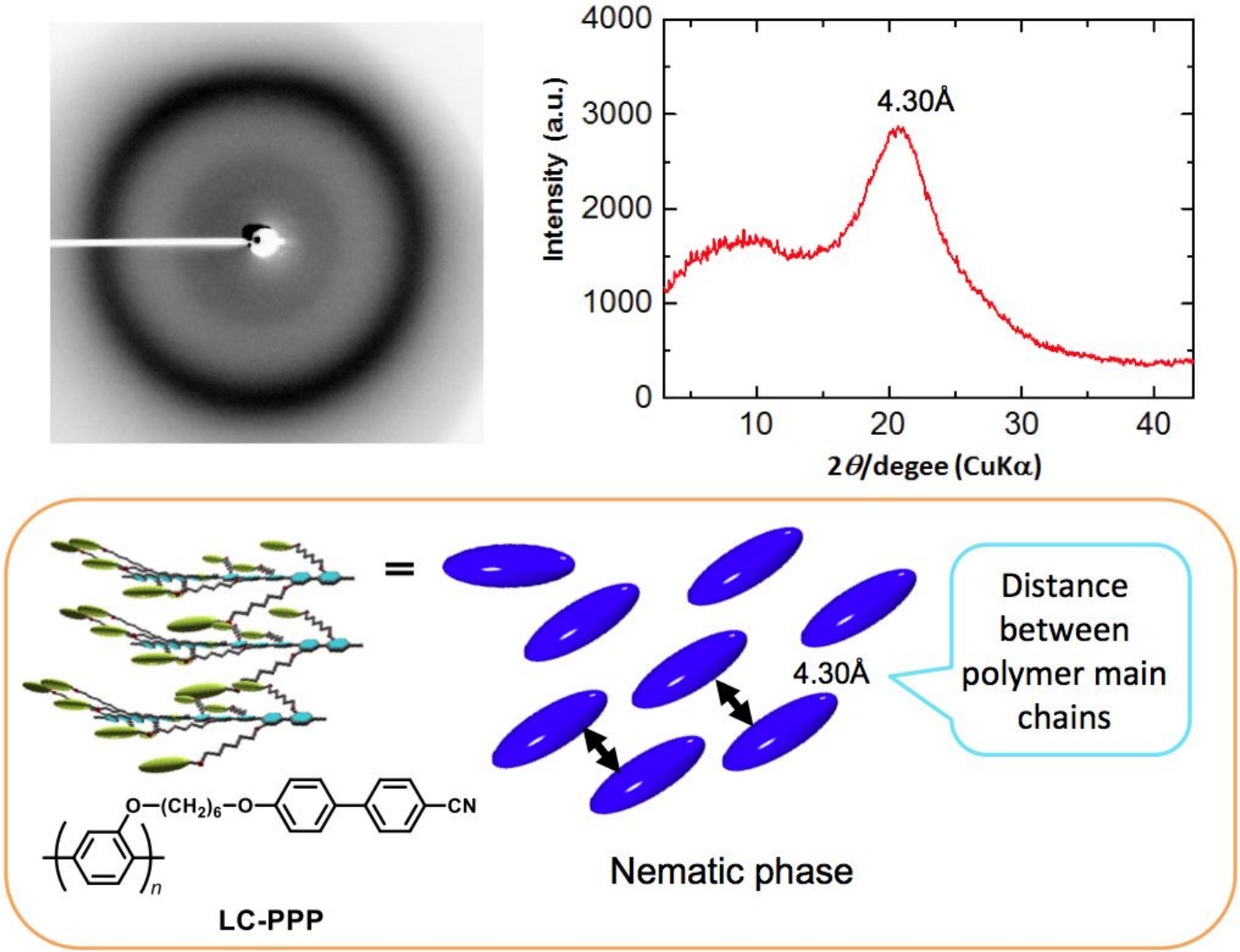

Fig. 3 (Upper) XRD pattern of LC-PPP in the annealed film and (lower) schematic of the nematic phase of LC-PPPs.

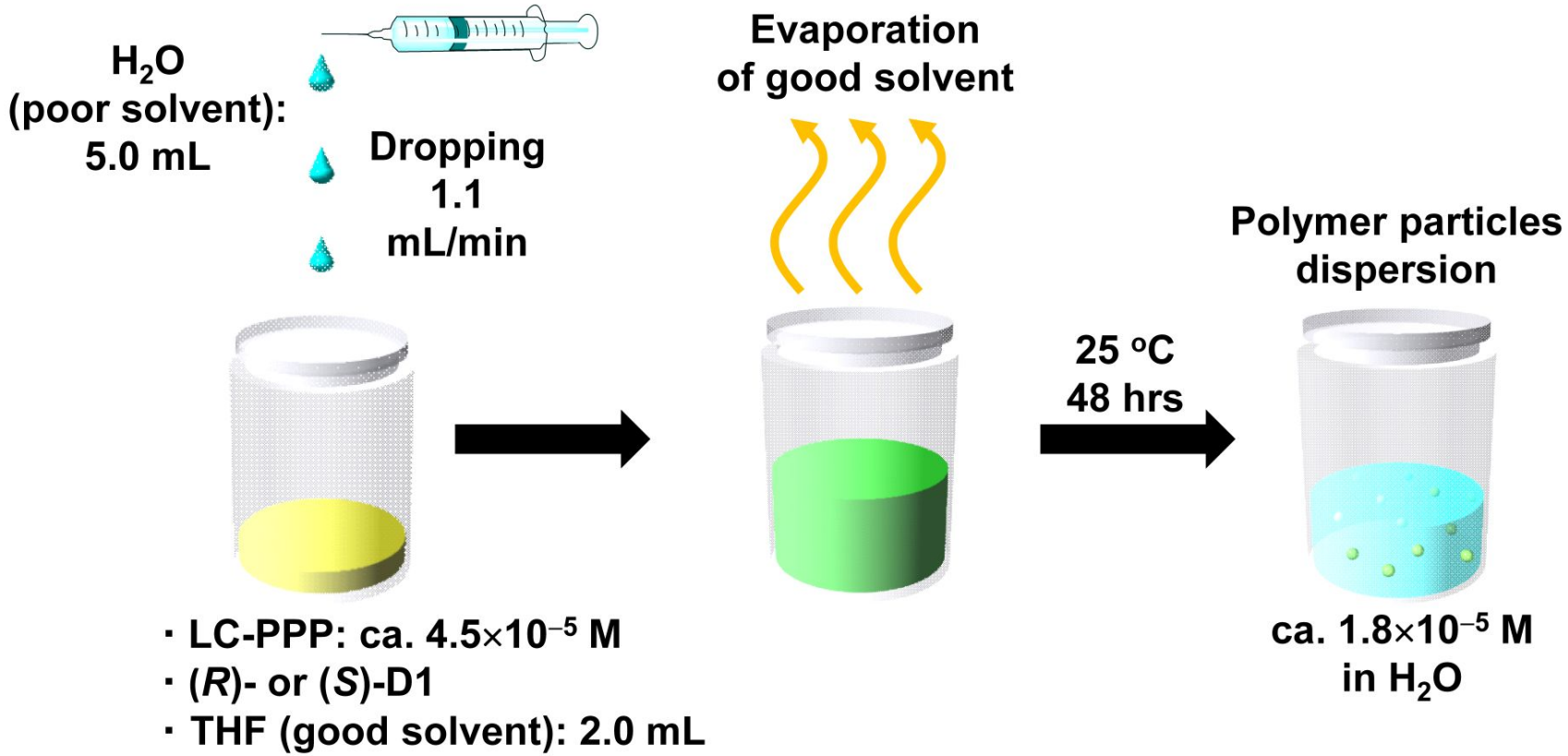

Fig. 4 Preparation of particle dispersion systems by the SORP method.

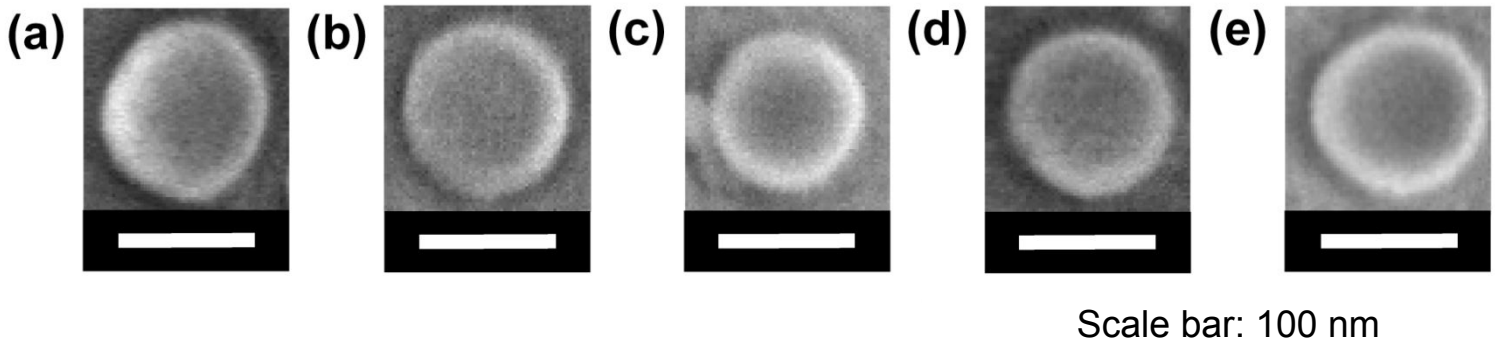

Fig. 5 SEM images of particles in (a) R10, (b) S1, (c) S2, (d) S5, and (e) S10.

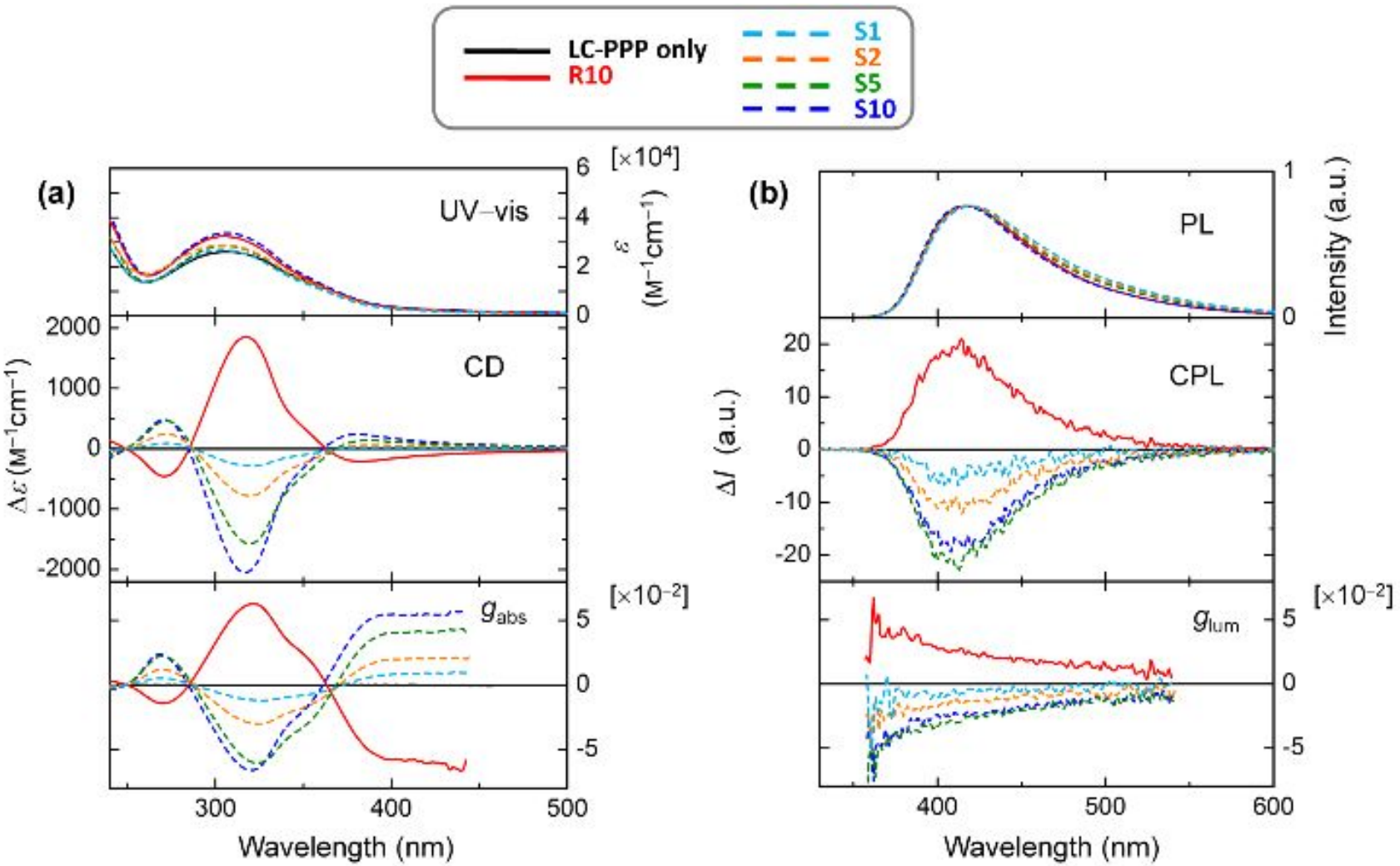

Fig. 6 (a) UV−vis and CD spectra and (b) PL and CPL spectra of the polymer-particle dispersion systems.

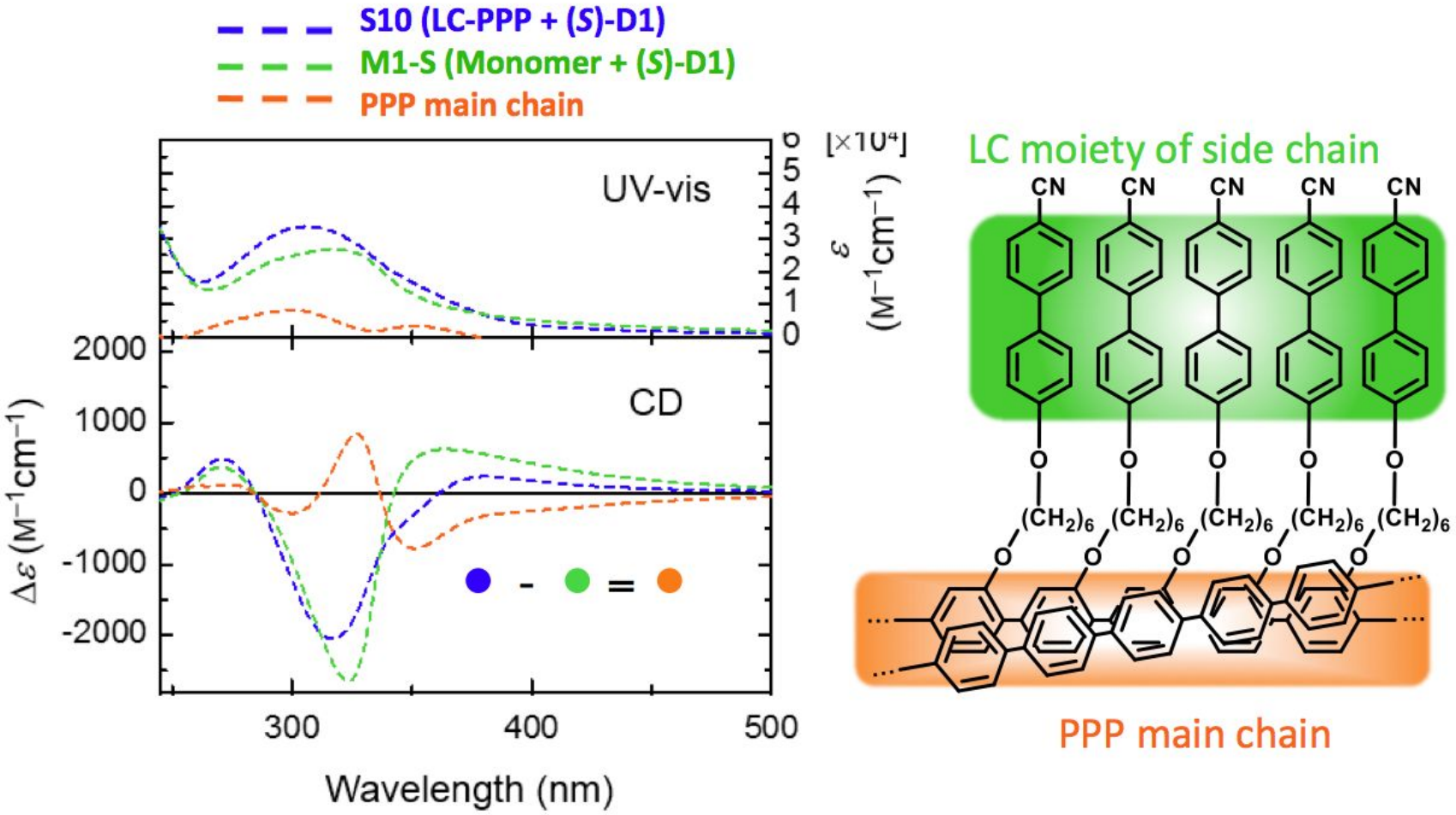

Fig. 7 UV−vis and CD spectra of the S10 and M1-S systems and the difference spectrum for the PPP main chain obtained by subtracting the M1-S spectrum from the S10 spectrum.

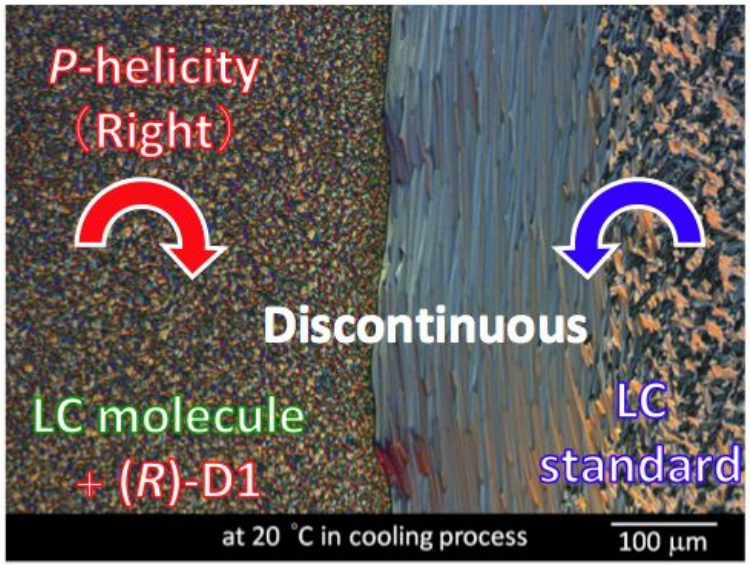

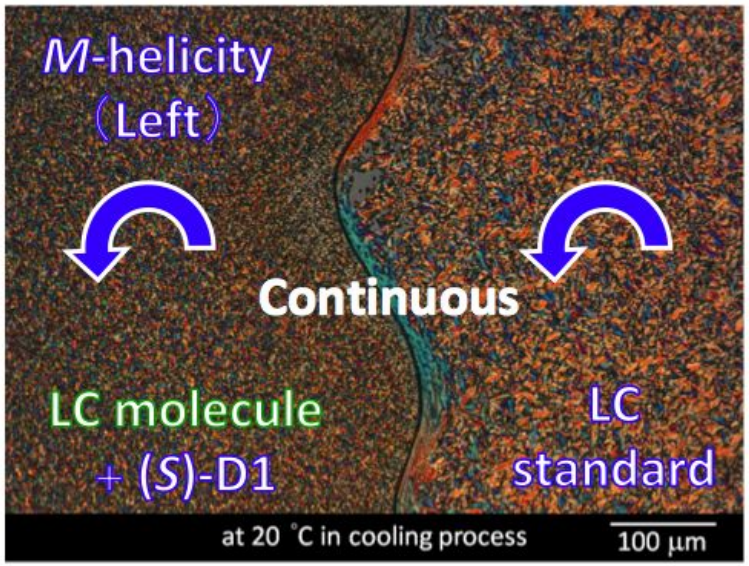

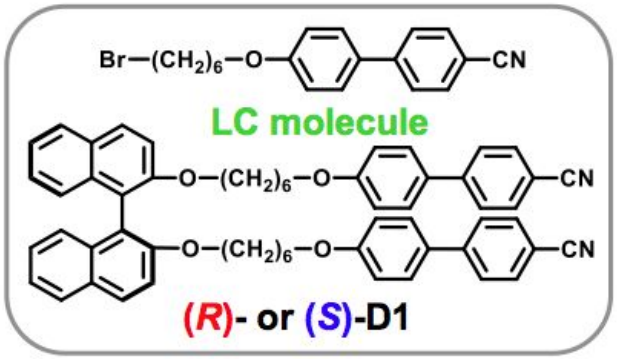

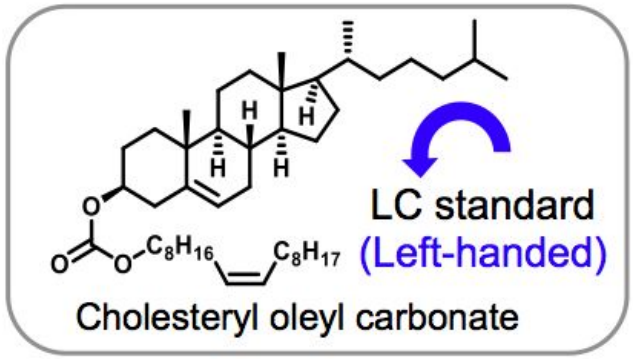

Fig. 8 Contact test between the mixture of LC molecule and chiral dopant (*R*)-/(*S*)-D1 and cholesteryl oleyl carbonate used as a left-handed LC standard.

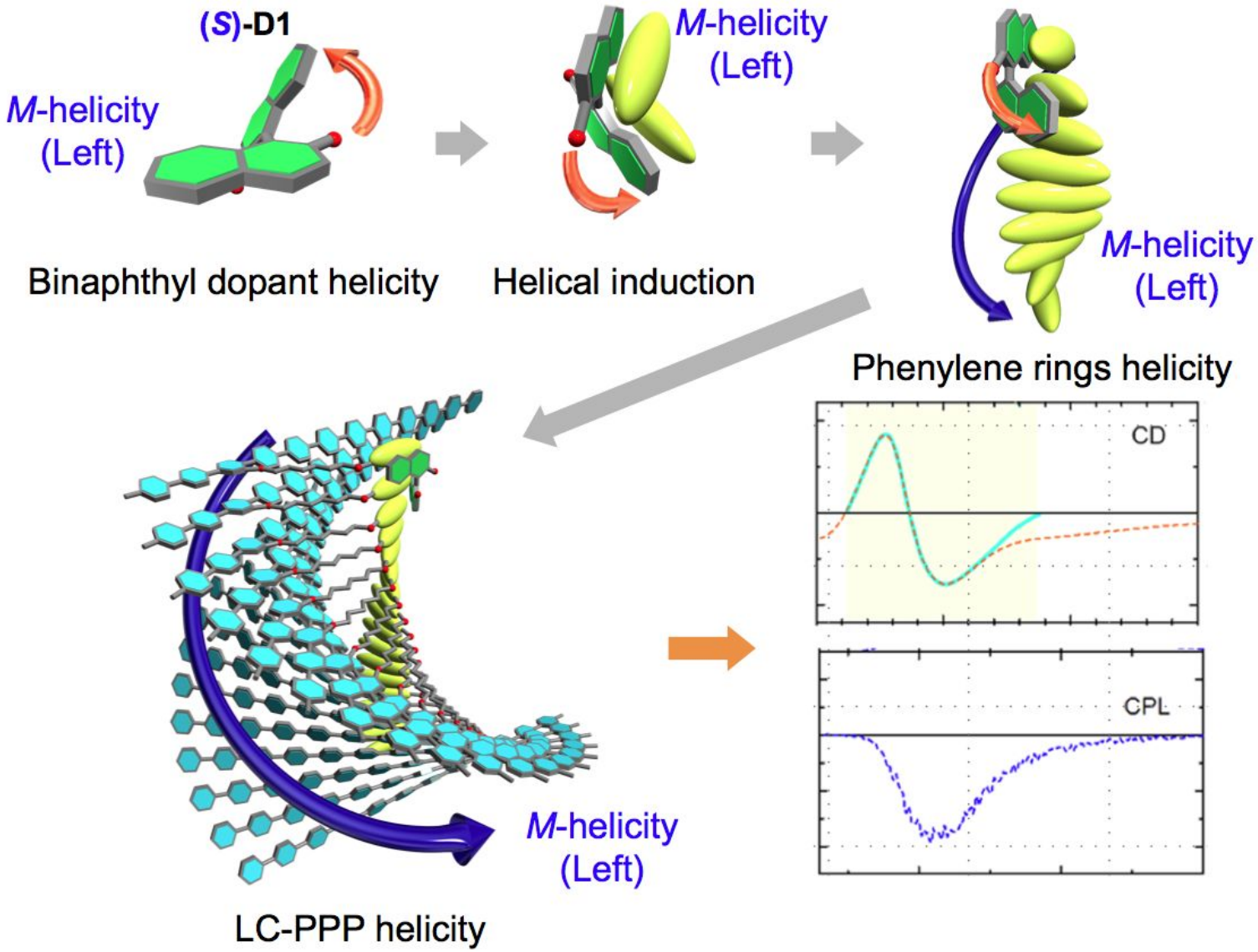

Fig. 9 Schematic of the mechanism of helicity transfer from (*S*)-D1 to the LC side chains of PPP.

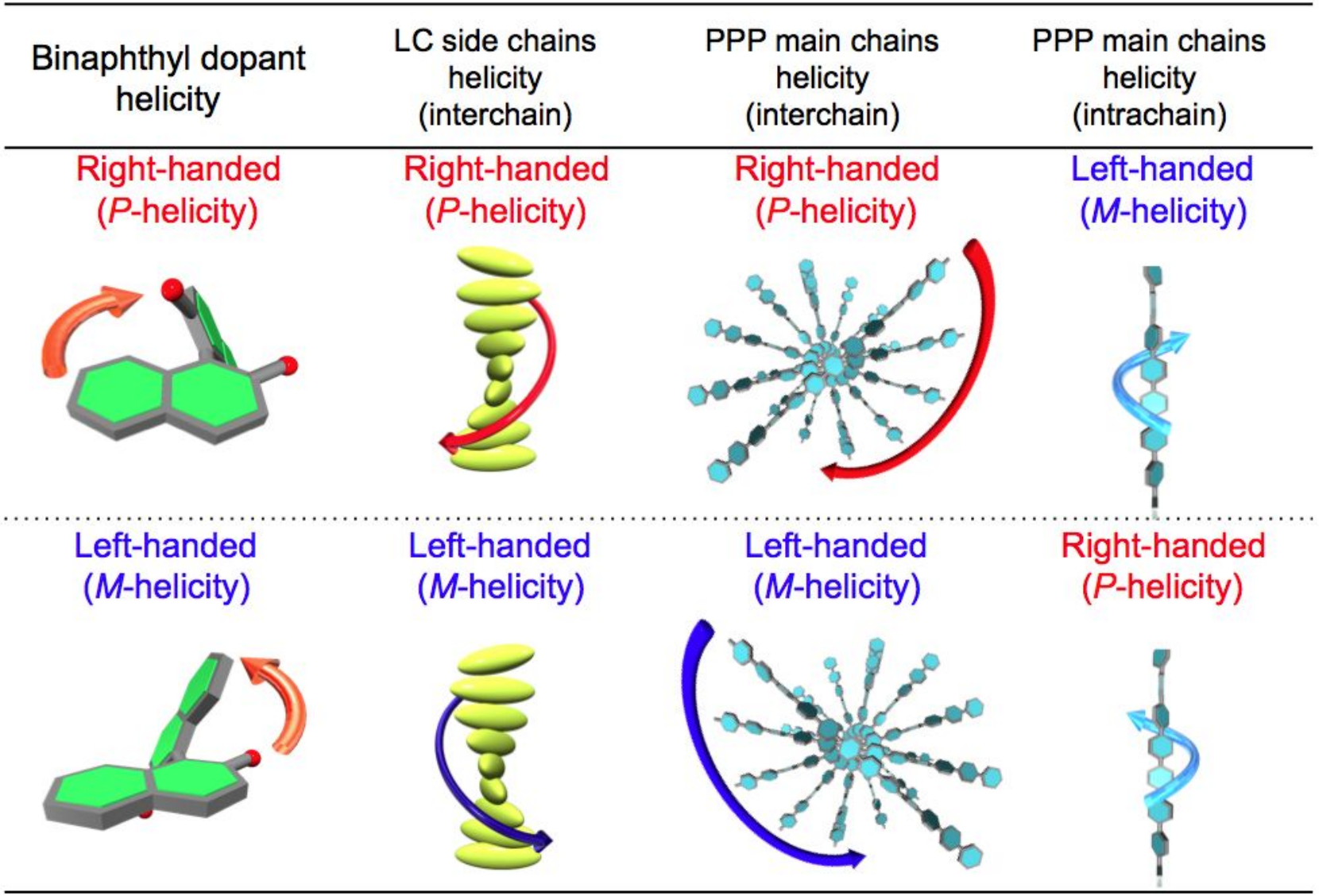

Fig. 10 Schematics showing helicity induced by the chiral dopant (*R*)-/(*S*)-D1 in different parts of LC-PPP.

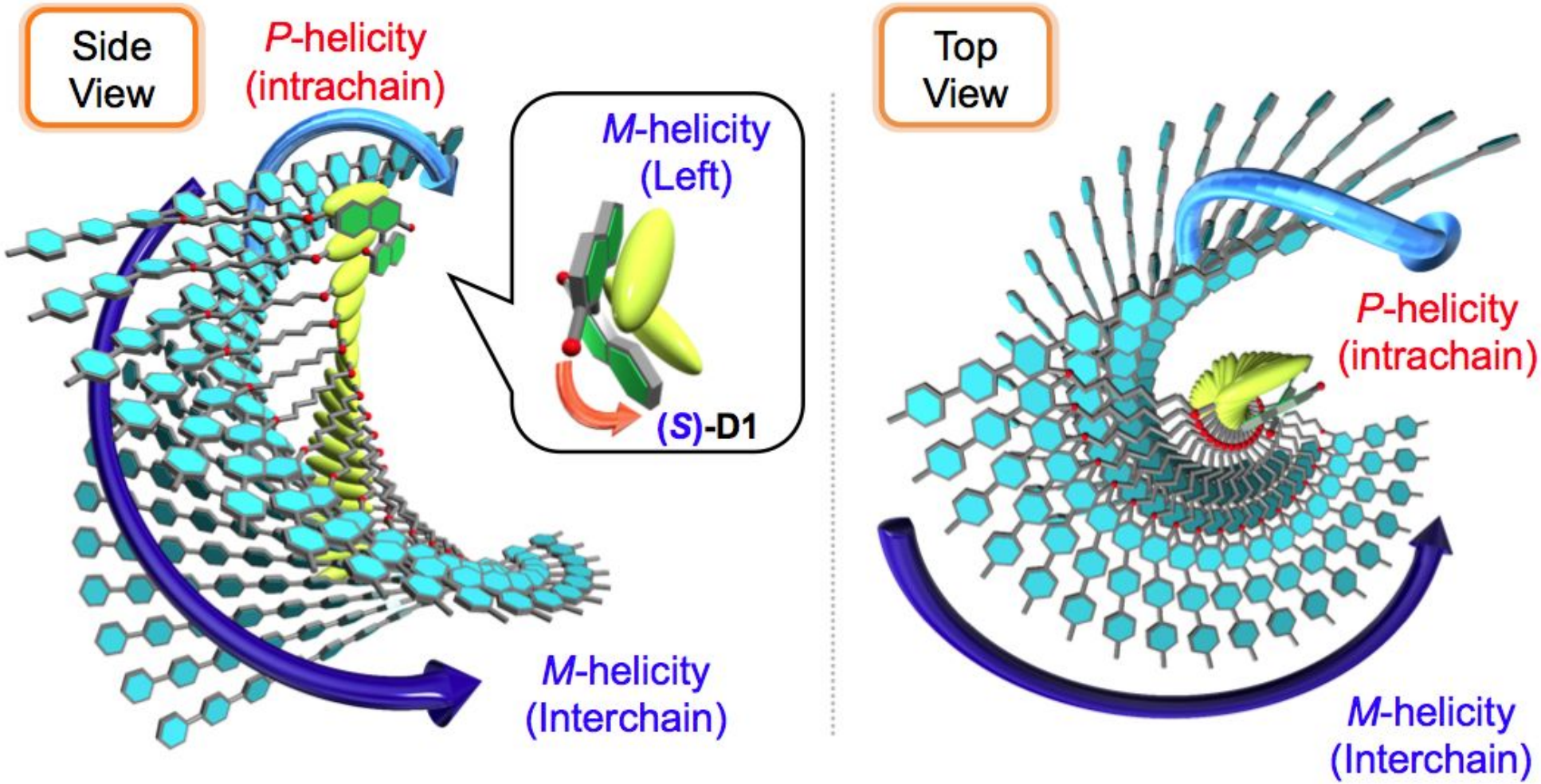

Fig. 11 Schematics showing helicity induced by the chiral dopant (*R*)-/(*S*)-D1 to the entire LC-PPP.

Table 1 Optical properties of LC-PPP and the chiral dopant (*R*)-/(*S*)-D1in $CHCl_3$ (2.0×10^{-5} M).

System	λ_{max} (nm)	$E_{m,max}$ (nm)	$E_{x,max}$ (nm)	Φ (%)[a]
LC-PPP	300	398	300	57.5
(*R*)-D1	296	362	297	16.1
(*S*)-D1	296	363	297	15.9

[a] Absolute quantum yield measured using integrating-sphere method.

Table 2 Conditions for the preparation of particle dispersion systems containing LC-PPP and (*R*)-/(*S*)-D1 by the SORP method.

System	configuration	Molar ratio LC-PPP:D1	Poor solvent	Good solvent	LC-PPP concentration	Evaporation time, temperature	Particle concentration
R10	*R*	100:10	H_2O (5.0 ml)	THF (2.0 ml)	ca. 4.5×10^{-5} M (in THF)	48 hrs, 25 °C	ca. 1.8×10^{-5} M (in H_2O)
S1	*S*	100:1					
S2	*S*	100:2					
S5	*S*	100:5					
S10	*S*	100:10					

Table 3 Optical properties of particle dispersion systems, including LC-PPP and the chiral dopant (*R*)-/(*S*)-D1.

System	λ_{max} (nm)	$E_{m,max}$ (nm)	$E_{x,max}$ (nm)	Φ (%)[a]	g_{abs}[b]	g_{lum}[c]
R10	317	422	306	14.5	$+6.11 \times 10^{-2}$	$+2.37 \times 10^{-2}$
S1	320	422	305	15.2	-1.16×10^{-2}	-4.71×10^{-3}
S2	319	422	306	9.9	-2.93×10^{-2}	-1.34×10^{-2}
S5	319	422	305	9.9	-5.88×10^{-2}	-2.36×10^{-2}
S10	317	422	305	10.0	-6.51×10^{-2}	-2.28×10^{-2}

[a] Absolute quantum yield measured using integrating-sphere method.

[b] Dissymmetry factor in absorption at λ_{max} wavelength.

[c] Dissymmetry factor in luminescence at $E_{m,max}$ (nm) wavelength.

Table 4 Conditions for the preparation of particle dispersion systems containing the M1 monomer and (*R*)-/(*S*)-D1 by the SORP method.

Systems	D1 configuration	Molar ratio M1:D1	Poor solvent	Good solvent	M1 concentration	Evaporation time, temperature	Particle concentration
M1-R	*R*	100:10	H_2O (5.0 ml)	THF (2.0 ml)	ca. 4.5 $\times 10^{-5}$ M (in THF)	48 hrs, 25 °C	ca. 1.8 $\times 10^{-5}$ M (in H_2O)
M1-S	*S*	100:10					